**Atmospheric
Chemistry
and Physics**

Heterogeneous oxidation of saturated organic aerosols by hydroxyl radicals: uptake kinetics, condensed-phase products, and particle size change

I. J. George[1], A. Vlasenko[1], J. G. Slowik[1], K. Broekhuizen[2], and J. P. D. Abbatt[1]

[1]Department of Chemistry and Southern Ontario Centre for Atmospheric Aerosol Research, University of Toronto, 80 St. George Street, Toronto M5S 3H6, Ontario, Canada
[2]Department of Chemistry, Colgate University, 13 Oak Dr., Hamilton, NY 13346, USA

Abstract. The kinetics and reaction mechanism for the heterogeneous oxidation of saturated organic aerosols by gasphase OH radicals were investigated under NO_x-free conditions. The reaction of 150 nm diameter Bis(2-ethylhexyl) sebacate (BES) particles with OH was studied as a proxy for chemical aging of atmospheric aerosols containing saturated organic matter. An aerosol reactor flow tube combined with an Aerodyne time-of-flight aerosol mass spectrometer (ToF-AMS) and scanning mobility particle sizer (SMPS) was used to study this system. Hydroxyl radicals were produced by 254 nm photolysis of O_3 in the presence of water vapour. The kinetics of the heterogeneous oxidation of the BES particles was studied by monitoring the loss of a mass fragment of BES with the ToF-AMS as a function of OH exposure. We measured an initial OH uptake coefficient of γ_0=1.3 ($\pm$0.4), confirming that this reaction is highly efficient. The density of BES particles increased by up to 20% of the original BES particle density at the highest OH exposure studied, consistent with the particle becoming more oxidized. Electrospray ionization mass spectrometry analysis showed that the major particle-phase reaction products are multifunctional carbonyls and alcohols with higher molecular weights than the starting material. Volatilization of oxidation products accounted for a maximum of 17% decrease of the particle volume at the highest OH exposure studied. Tropospheric organic aerosols will become more oxidized from heterogeneous photochemical oxidation, which may affect not only their physical and chemical properties, but also their hygroscopicity and cloud nucleation activity.

1 Introduction

Atmospheric aerosols play an important role in atmospheric chemistry, climate, visibility, and human health (Seinfeld and Pandis, 1998; Finlayson-Pitts and Pitts, 2000; Ramanathan et al., 2001). Knowing that organic matter can make up a significant fraction of tropospheric aerosol (Jacobson et al., 2000; Saxena and Hildemann, 1996), the question arises as to whether atmospheric organic particles can be chemically transformed by heterogeneous reactions with gas-phase oxidants such as O_3, OH, Cl and NO_3. Chemical aging of organic particles from heterogeneous oxidation modifies particle physico-chemical properties such as size, morphology, composition, hygroscopicity, and ability to act as cloud nuclei. Therefore, aging may significantly impact the role of organic aerosols on climate, atmospheric chemistry and other relevant environmental processes. Despite the importance of chemical aging of atmospheric organic aerosols, our current understanding of this process is limited.

Recently, there has been a focus of research on understanding the chemical transformation of atmospheric organic aerosol. Laboratory research has concentrated on the reaction of O_3 with condensed-phase unsaturated organic compounds, e.g., oleic acid, as a proxy for chemical aging of organic aerosol (e.g., Moise and Rudich, 2002; Morris et al., 2002; Hearn and Smith, 2004; Katrib et al., 2004; Thornberry and Abbatt, 2004; Hearn and Smith, 2005; Katrib et al., 2005; Knopf et al., 2005; Ziemann, 2005). Fewer studies have been conducted to investigate the chemical aging of condensed-phase saturated organics by atmospheric radicals (e.g., Bertram et al., 2001; Moise and Rudich, 2001; Eliason et al., 2004; Molina et al., 2004; Hearn and Smith, 2006; Knopf et al., 2006; Hearn et al., 2007; Lambe et al., 2007).

OH is the most efficient atmospheric oxidant in the troposphere, and therefore, it is expected to play an important role in chemical aging of atmospheric condensed organic matter.

Correspondence to: J. P. D. Abbatt
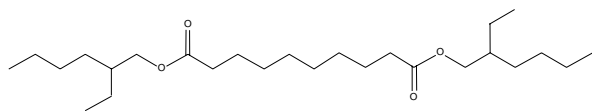(jabbatt@chem.utoronto.ca)

Fig. 1. Chemical structure of Bis(2-ethylhexyl) sebacate (BES).

Several studies have shown that the reaction of organic surfaces with OH is highly efficient compared to reaction with other radicals such as NO$_3$ (Moise et al., 2002; Knopf et al., 2006) and Cl (Moise and Rudich, 2001), with OH reactive uptake probabilities anging from 0.2 to 1 (Cooper and Abbatt, 1996; Bertram et al., 2001; Molina et al. 2004). A few attempts have been made to elucidate the reaction mechanism for the heterogeneous reaction of OH with organic surfaces by observing reaction products. Molina et al. (2004) observed complete volatilization of alkane monolayers from reaction with OH, indicating that heterogeneous oxidation of organic aerosol by OH leads to the release of oxygenated volatile organic products into the troposphere. Molina et al. (2004) further suggest that volatilization from chemical aging by reaction with OH may be as important as wet deposition as a removal pathway for organic aerosols in the lower atmosphere. However, other studies suggest that the reaction pathway leading to release of volatile products from the oxidation of organic surfaces by OH plays a minor role in the reaction mechanism. A more recent study by Knopf et al. (2006) found that oxidation of alkane monolayers by atmospheric exposures of NO$_3$ leads to volatilization of no more than 10% of the surface. Moise and Rudich (2001) measured 20% carbon loss from an alkane monolayer due to reaction with halogen radicals. The results from these studies contrast with the Molina et al. (2004) findings, even though the oxidation of a saturated organic surface by Cl or NO$_3$ is expected to proceed through a similar reaction mechanism as oxidation by OH. Therefore, the importance of volatilization resulting from the oxidation of atmospheric saturated organic matter by OH is currently still unclear.

The study of condensed-phase products from heterogeneous oxidation of saturated organic surfaces has been largely restricted to X-ray photoelectron spectroscopy (XPS) analysis of oxidized alkane monolayer surfaces, which provides information on the degree of oxidation and on the presence of oxidized functional groups (Moise and Rudich, 2001; Molina et al., 2004; Knopf et al., 2006). Eliason et al. (2004) reported the formation of condensed-phase ketones and short-chained aldehydes from the reaction of OH with hexadecane film using GC-MS analysis. Although these studies suggest that atmospheric organic aerosols should become more oxidized from chemical aging, this has not yet been confirmed in the laboratory with saturated organic aerosols. Laboratory studies involving the oxidation of organic surfaces by OH have typically used organic monolayers or films as proxies for organic particles, even though the

greater physical and chemical complexity of particles may influence the aging process. Further, there have been no efforts to simultaneously characterize both gas- and particle-phase products from the heterogeneous reaction of OH with organic surfaces or particles. Therefore, because of the uncertainties mentioned above, the reaction mechanism for this process is not fully understood.

To address the gaps in knowledge of the aging process of organic particles, we investigate the heterogeneous reaction of organic aerosols with OH under NO$_x$-free conditions using online particle analysis techniques. The experimental NO$_x$-free conditions in this study were chosen as an initial simplified case, which simulates atmospheric conditions in remote regions. Bis(2-ethylhexyl) sebacate (C$_{26}$H$_{50}$O$_4$, BES) aerosols were selected as a proxy for atmospheric aerosol containing saturated organic matter. The chemical structure of BES is shown in Fig. 1. Because of its structure, BES has several properties that make BES particles a good proxy for organic aerosols in this laboratory study. BES has a very low vapour pressure (2.8×10^{-6} Pa at 25°C) to minimize gas-phase reactions with OH. It also contains no unsaturated moieties and, therefore, will not react with O$_3$. Further, BES particles are liquid at room temperature eliminating complications of particle shape on particle analysis. The use of liquid organic aerosols allows for the study of heterogeneous kinetics including surface and bulk particle processes more closely mimicking aging processes occurring in organic aerosols unlike the study of organic films.

The heterogeneous reaction of BES particles with OH was studied in an aerosol reactor flow tube coupled to an Aerodyne time-of-flight aerosol mass spectrometer (ToF-AMS). There are four major objectives of this study: 1) measure the kinetics of the heterogeneous reaction of OH with BES particles by observing the reactive loss of particle-phase BES, 2) determine the effect of the reaction on the particle physical properties (particle size, density, and extent of volatilization), 3) characterize the particle-phase products, and 4) elucidate the reaction mechanism. This study focuses on the identification of condensed-phase products, while a future paper (Vlasenko et al., 2007[1]) will discuss the characterization of volatilized products.

2 Experimental

2.1 Aerosol reactor flow tube setup

The experimental system used to study the heterogeneous oxidation of BES particles is shown in Fig. 2. BES particles were generated by homogeneous nucleation by passing 0.3 slpm flow of N$_2$ (BOC, 99.998%) through a Pyrex tube

---

[1]Vlasenko, A., George, I., and Abbatt, J. P. D.: Formation of volatile organic compounds in the heterogeneous oxidation of condensed phase organic films by gas-phase OH, in preparation, 2007.
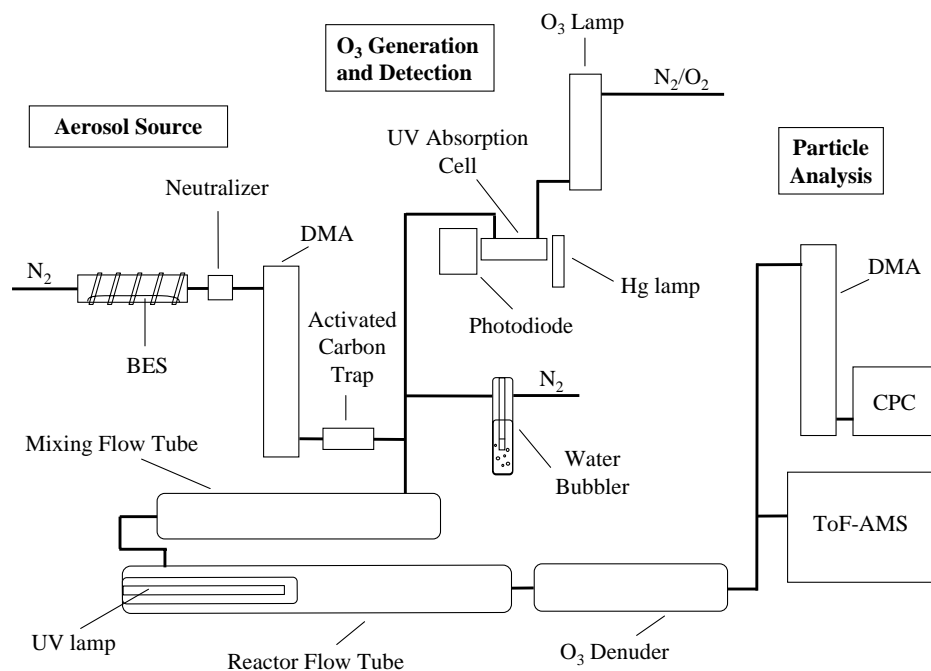
Fig. 2. Aerosol flow reactor setup for the study of the heterogeneous oxidation of organic aerosols.

containing liquid BES (Fluka, >97%), that is heated to approximately 110°C. The aerosol flow passed through a neutralizer (TSI model 3077), and the particles were then size-selected to monodisperse aerosol with a mode mobility diameter (D_m) of D_m=150 nm by a differential mobility analyzer (DMA) column (TSI model 3081). The ratio of sheath to sample flow rates in the DMA was held at a constant value of 10. The monodisperse aerosol then passed through an activated carbon trap to remove volatile organics from the flow.

OH radicals were produced by the photolysis of O_3 in the presence of water vapour as follows. O_3 was generated by passing a mixture of N_2 and O_2 (BOC, 99.994%) through an O_3 generator (Jelight model 1000). O_2 concentrations in the flow tube ranged from approximately $[O_2]=5\times10^{16}$–5×10^{18} molecules cm^{-3}. In general, O_2 concentrations positively correlated with O_3 concentrations and OH exposures. The influence of O_2 concentration on the reaction was examined by adjusting the O_2 concentrations at fixed OH exposures by the addition of a pure O_2 flow to the ozone flow. O_3 concentrations were monitored before entering the aerosol reactor flow tube by measuring absorbance at 254 nm in a 14 cm long UV absorption cell. The O_3 flow was mixed with a humidified N_2 flow that had passed through a water bubbler. The humidified O_3 and aerosol flows having a total volumetric flow rate of approximately 0.7 slpm were passed into a mixing flow tube 0.8 L in volume. The mixed humidified O_3/aerosol flow was then introduced into the reactor flow tube that was at 1 atm and room temperature of 24°C. The mixture was illuminated in the flow tube by a 22.9 cm O_3-free Hg Pen-ray

lamp (UVP) inside the reactor flow tube. The UV lamp had a primary energy output at 254 nm and was surrounded by a Quartz sheath tube that was purged with compressed air to cool the lamp. The UV lamp housing was treated to filter out 185 nm light to prevent O_3 production by the lamp. The average reaction time of OH with the BES particles was calculated from the illuminated volume (V=0.87 L) and the flow rate. An O_3 denuder was placed downstream of the reactor flow tube to destroy the O_3 in the flow. After passing through the O_3 denuder, the reacted particles were analyzed (see Sects. 2.3 and 2.4).

2.2 OH quantification

The steady-state OH concentrations were calculated in each experiment with a photochemical model using the Acuchem program (Braun et al., 1988). Experimental inputs into the model were O_3 and H_2O concentrations in the reactor flow tube. The O_3 concentrations in the reactor flow tube, with the range of $[O_3]=0$–3×10^{15} molecules cm^{-3}, were determined from the O_3 concentrations at the O_3 detector (see Fig. 2) and the volumetric flow rates of the O_3 flow and total mixed flow. The relative humidity of the flow exiting the reactor flow tube was measured with a hygrometer (VWR, ±1%) and varied between approximately 30 and 60%.

The Acuchem model included gas-phase reactions involved in the production of OH from O_3 and water vapour and major OH loss reactions with kinetic rate constants associated with these reactions taken from DeMore et al. (1997). The model was validated in our laboratory by comparing

modelled OH concentrations to measured OH concentrations under varying experimental conditions. Steady-state OH concentrations were measured during the model validation experiments by reacting OH with SO$_2$ (Matheson, 99.98%) in the reactor flow tube. The decay of SO$_2$ from its reaction with OH was measured using a chemical ionization mass spectrometer (CIMS) in negative ion mode using SF$_6^-$ as the reagent ion. The CIMS setup has been previously described in detail by Thornberry and Abbatt (2004).

The extent of decay of SO$_2$ from its reaction with OH was determined by monitoring intensity of the m/z 102 ion peak corresponding to F$_2$SO$_2^-$ ion, a product of the reaction of SF$_6^-$ with SO$_2$. We measured the change in SO$_2$ signal due to the illumination of the humidified O$_3$/SO$_2$/aerosol flow compared to dark reactor flow tube conditions. The OH concentration was determined from the decay of SO$_2$ signal intensity using a rate constant for the reaction OH + SO$_2$ calculated from DeMore et al. (1997). Control experiments showed that SO$_2$ levels were not affected individually by H$_2$O, O$_3$, or UV lamp; SO$_2$ levels only declined when all were present. Two model parameters were adjusted to fit the measured OH concentrations: the photolysis rate constant for O$_3$ (J$_{O3}$) and an OH wall-loss rate constant (k$_{wall}$). The model predictions deviated from the measured values by less than ±24% after these adjustments are made. Note that SO$_2$ was present only for the experiments to validate the OH model; it was absent when the aerosol oxidation experiments were conducted.

2.3 Kinetic experimental methods

The kinetics of the heterogeneous reaction of OH with BES particles in the aerosol flow reactor were investigated by measuring the loss of particle-phase BES as a function of OH exposure ranging from 0 to 9×10^{-8} atm-s. As shown in Fig. 2, the reacted particle flow was split after the O$_3$ denuder and the particles were analyzed by a scanning mobility particle sizer (SMPS) and an Aerodyne time-of-flight aerosol mass spectrometer (ToF-AMS). The SMPS, including electrostatic classifier (TSI model 3080), neutralizer (TSI model 3076), DMA column (TSI 3081) and condensation particle counter (TSI model 3025), measured the reacted particle size distribution over the mobility diameter range D$_m$=50 to 300 nm with a scan time of 2.5 min. The ToF-AMS provided size-resolved chemical composition of the reacted particles and particle mass distributions in terms of vacuum aerodynamic size diameter. The ToF-AMS instrument has been described in detail elsewhere (Drewnick et al., 2005). For the kinetic studies, 10 min averaged measurements of the unreacted particles and reacted particles were compared. All measurements were normalized to SMPS particle number concentration to compensate for variations in particle generation stability. Under unreacted particle conditions (referred to as I$_0$), the aerosols were entrained in a flow of N$_2$, O$_2$, and water vapour with the UV lamp on continuously, but O$_3$ was

absent. The conditions under which particles are reacted (referred to as I) differed from I$_0$ only in that the O$_3$ generator was turned, producing OH in the reactor flow tube. Control experiments showed that exposing BES particles to O$_3$ or the UV lamp individually did not affect the particle composition or size within experimental error.

2.4 Product characterization methods

Several techniques were used to analyze the composition of the condensed-phase and gas-phase reaction products. The ToF-AMS provided the mass spectrum of the reacted particles, and the major mass fragments yield structural information about the condensed-phase reaction products. However, due to the nature of the ToF-AMS ion source (electron impact at 70 eV), fragmentation of the reaction products was too extensive to permit detection of the molecular ion. To obtain the molecular ions, the particle-phase products were also analyzed by a Micromass QTOF Ultima mass spectrometer (ESI-MS). This instrument utilizes an electrospray ionization (ESI) source that is sufficiently soft to preserve the molecular ion peaks of the product. To prepare samples for ESI-MS analysis, polydisperse BES aerosol with a mode diameter of 146 nm (σ_g=1.4) and number concentration of 3.6×10^6 cm^{-3} was oxidized and collected for approximately 3 h onto a glass fiber filter (GF/A 47 mm, Whatmann). A control sample was prepared by collecting BES particles under unreacted particle conditions for 1 h. Filters were extracted with approximately 10 mL of methanol (Fisher, HPLC grade) in amber vials and sonicated for 30 min. The extracts were transferred to clean vials and concentrated to 1 mL under a flow of N$_2$.

3 Results and discussion

3.1 Kinetic studies

We studied the kinetics of the heterogeneous oxidation of BES particles by gas-phase OH radicals in a NO$_x$–free environment by monitoring the intensity of a mass fragment characteristic to BES with the ToF-AMS. Figure 3a shows the ToF-AMS mass spectrum of unreacted BES particles. Due to extensive fragmentation of organic molecules in the ToF-AMS, the molecular ion for BES at m/z 426 was not observed in the ToF-AMS mass spectrum, even when the electron energy was lowered from 70 eV to 20 eV. This is consistent with results reported earlier by Alfarra (2004). Instead, several mass fragments characteristic of BES were monitored including the marked peaks in Fig. 3a. In Fig. 3b, the mass spectrum of the reacted particles clearly shows that these BES fragments have decreased in intensity. Note that the mass intensities shown in Figs. 3a and b have been normalized to the same particle number concentration. We found that the mass fragment m/z 297 had the fastest decay rate as a function of OH exposure, indicating that it is least likely to
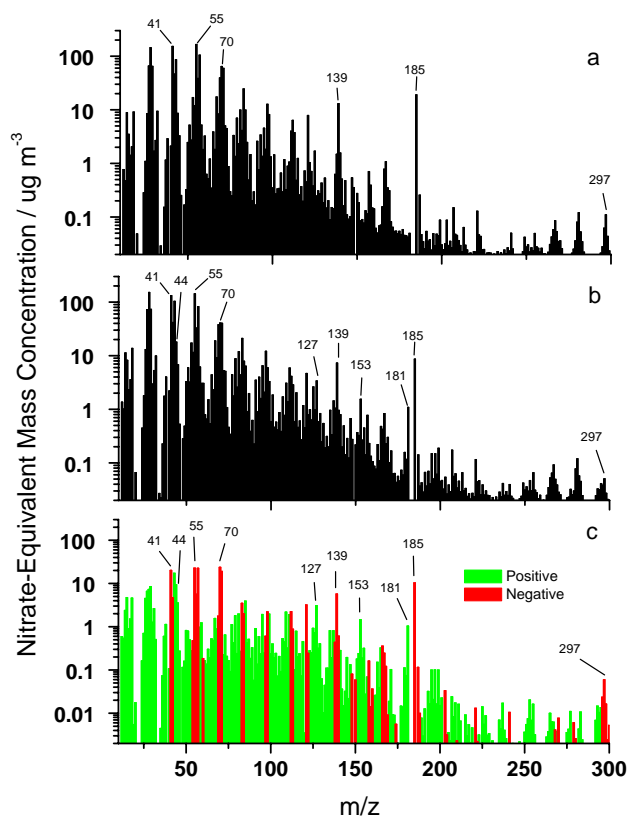
Fig. 3. ToF-AMS mass spectra of BES particles normalized to same particle number concentration: **(a)** unreacted particles, **(b)** reacted particles at OH exposure of 2.7×10^{-8} atm-s, **(c)** difference spectra of reacted spectrum minus unreacted spectrum, with positive values shown in green and negative values shown in red.

be a fragment of the particle-phase products. Furthermore, the rate of loss of m/z 297 had yielded a comparable rate constant value to that of the formation of several primary product peaks (see Sect. 3.3), validating our assumption that mass 297 has similar decay kinetics to BES. Therefore, the decay of the m/z 297 fragment was monitored as a function of OH as a proxy for the reactive loss of particle-phase BES. In Fig. 4, the relative change in signal at m/z 297 is plotted as a function of OH exposure (atm-s). The experimental conditions for I and I_0 were described earlier in the Experimental section. We note that the precision of the m/z 297 signal was 5% for a ten minute timescale in the absence of OH.

The measured reactive uptake coefficient (γ) for the reaction of OH with BES particles is defined here as the fraction of OH collisions with the particle surface leading to reactive loss of particle-phase BES. We make an assumption that the reactive loss rate of particle-phase BES is equal to the rate of OH reaction with BES. The validity of this assumption will be discussed below. As shown in Fig. 4, the rate of decay of m/z 297 signal decreases at high OH exposures. The reactive uptake coefficient will decrease at high OH concentra-
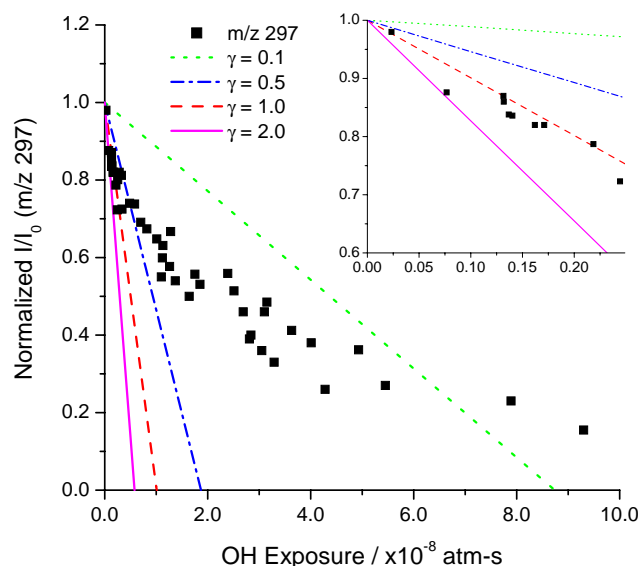

Fig. 4. Change in m/z 297 signal intensity as a function of OH exposure. Experimental data are shown as square symbols, and solid lines show calculated slopes using Eq. (1) with γ_0 values of 0.1 (green dotted), 0.5 (blue dash-dotted), 1.0 (red dashed), and 2.0 (pink solid) Inset is a magnification of the plot showing the data used for calculation of γ_0.

tions as the surface concnetrations of condensed-phase BES decrease and OH increasingly reacts with particle products. Therefore, we will focus on the determination of the initial reactive uptake coefficient (γ_0, where γ_0 is defined as γ extrapolated to zero OH exposure, which can be considered an upper limit for γ.

The initial reactive uptake coefficient (γ_0 of OH with BES particles was calculated using the formulation in Katrib et al. (2005):

$$\gamma_0 = \frac{-d\left([I_{297}]/[I_{297}]_0\right)}{d\left([OH]\,t\right)} \frac{V}{A} \frac{4RT}{\bar{c}} [BES]_0 \qquad (1)$$

Here, the first term is the slope of the linear fit of the experimental data in Fig. 4, V/A is the particle volume to surface area ratio (particle diameter/6 for the spherical particles used in this study), $\bar{c}$ is the mean speed of gas-phase OH molecules, R is the gas constant, T is the temperature and $[BES]_0$ is the initial condensed-phase BES concentration. As mentioned before, the signal at m/z 297 is used as a proxy for [BES]. To calculate γ_0 from Eq. (1), the slope of a subset of the experimental data in Fig. 4 with OH exposures less than 2.5×10^{-9} atm-s was used. The experimental data used to calculate γ_0 are shown in the inset of Fig. 4. This cutoff point was chosen because the inclusion of further data at higher OH exposure significantly reduced the γ_0 value and the correlation coefficient of the linear fit of the experimental data in Fig. 4, from which the slope was determined.

The value of γ_0 calculated from experimental measurements using Eq. (1) was corrected for gas-phase diffusion
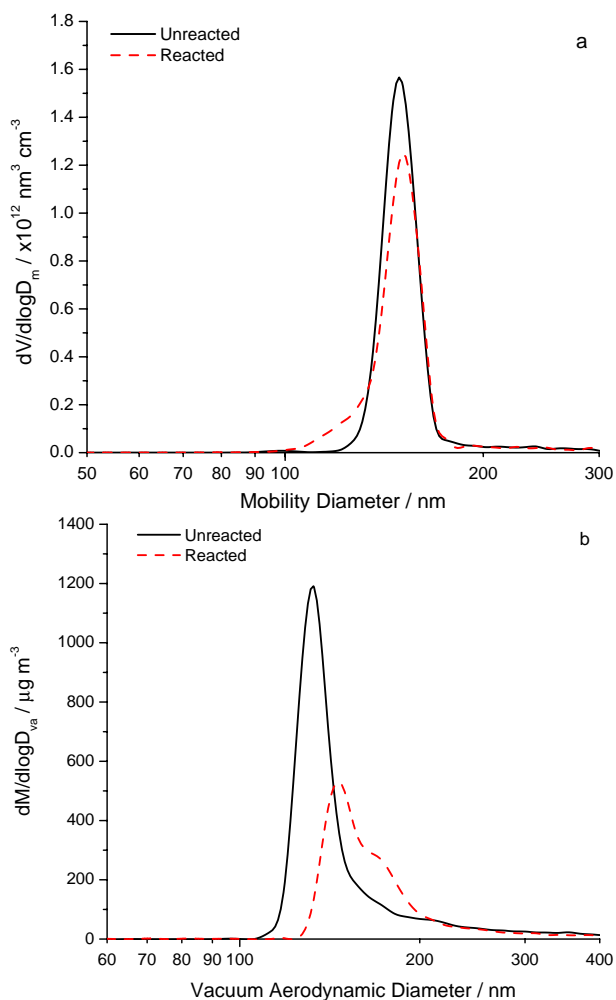
Fig. 5. Size distributions for unreacted (black solid line) and reacted (red dashed line, OH exposure=5.0×10^{-8} atm-s) BES particles normalized to the same particle concentrations: **(a)** DMA volume-weighted particle concentration as a function of mobility diameter. **(b)** ToF-AMS nitrate-equivalent mass concentration as a function of vacuum aerodynamic diameter.

by applying an empirical formulation by Fuchs and Sutugin (Fuchs and Sutugin, 1970; Worsnop et al., 2002). The gas-phase diffusion coefficient of OH (D_{OH}) needed for this calculation has not been measured in N_2, O_2, or H_2O. Therefore, we used gas-phase diffusion values of H_2O in N_2, O_2, and H_2O as an approximation for OH (Massman, 1998), which was calculated to be D_{OH}=0.260 cm^2 s^{-1} for our flow conditions. This value is close to the experimental D_{OH} value measured in dry air (Ivanov et al., 2007).

The solid lines in Fig. 4 represent slopes calculated from Eq. (1) using diffusion-corrected γ_0 values ranging from 0.1 to 2. It is clear from the inset in Fig. 4 that a diffusion-corrected γ_0 value close to 1 best fits the initial data used to calculate the experimental γ_0 value. The diffusion-corrected

initial reactive uptake coefficient value was calculated to be γ_0=1.3 ($\pm$0.4). The reported error is one standard deviation of the overall experimental error ($\pm$30%). Due to the high uptake coefficient, the diffusion correction was significant, with the adjustment being approximately 35%. Our γ_0 value is similar to those obtained in studies of the reactive uptake of OH on organic films and monolayers, where γ_0 values ranging from 0.2 to 1 have been measured (Cooper and Abbatt, 1996; Bertram et al., 2001; Molina et al., 2004). It should be noted that these studies determined γ by measuring the reactive loss of OH in the gas-phase as opposed to measuring the loss of particle-phase species as in our study. In the first case, γ must be by definition less than or equal to unity. In contrast, the latter case may lead to γ values that are greater than unity when secondary condensed-phase chemistry is an important loss mechanism for condensed-phase species. For example, Hearn and Smith (2006) measured γ_0=2.0 for OH oxidation of BES particles, which is somewhat larger than our value. From their results, Hearn and Smith (2006) suggested that OH-initiated secondary chemistry lead to additional loss of BES. Within our experimental uncertainties, we do not see a strong indication of such secondary chemistry, but we cannot rule out the possibility either. In a recent smog chamber study, Lambe et al. (2007) studied the reaction of hexacosane particles with OH using lower OH concentrations ([OH]=4–7×10^6 molecules cm^{-3}) and calculated a γ value of γ=1.04, which is in agreement with our γ_0 value .

3.2 Particle size and density modification

The SMPS and ToF-AMS were used in tandem in order to gain information on the particle size and density changes arising from the oxidation of organic aerosol by OH. These changes may indicate whether this reaction leads to release of oxygenated volatile organics from the particles. As suggested by Molina et al. (2004), volatilization from heterogeneous oxidation may be a significant atmospheric sink for particle-phase organic matter. Figure 5a shows the SMPS volume distributions as a function of mobility diameter for unreacted and reacted (OH exposure $\sim$5$\times10^{-8}$ atm-s) BES particles normalized to the same particle number concentration. Both volume distributions have approximately the same mode mobility diameter (D_m=151 nm) and both are relatively monodisperse. The reacted particle size distribution shows a slight decrease in concentration of particles with D_m=150 nm and corresponding increase in smaller particles with D_m=100–130 nm. The mean number-weighted mobility diameter decreased from 148 to 142 nm. For an OH exposure of 5×10^{-8} atm-s, total particle volume normalized for particle concentration decreased by 7%, even though the signal intensity at m/z 297 decreased by 70% at this exposure.

In Fig. 5b, the ToF-AMS total organic mass distributions for the unreacted and reacted aerosol populations are displayed as a function of vacuum aerodynamic diameter (D_{va}). The mass particle distribution shifted from a mean

D_{va}=133 nm to 148 nm at an OH exposure of 5×10^{-8} atm-s. The reaction-induced increase in vacuum aerodynamic diameter and corresponding decrease in mobility diameter suggests that the particle density increases as a result of OH exposure. Typically, oxygenated organic species have higher material densities than hydrocarbon species. It is therefore likely that the density of reacted particles would increase with oxidation if the oxidized products remain in the condensed phase. The particle density of reacted BES was determined using the following equation (DeCarlo et al., 2004):

$$\rho_p = \frac{D_{va}}{D_m} \rho_0 \qquad (2)$$

where ρ_p is the particle density and ρ_0 is the standard density (ρ_0=1.0 g cm^{-3}). Equation (2) is valid only for spherical particles with no voids, which is the case for the liquid BES particles used in this study. We confirmed that the particles remained spherical even after reaction by measurement of the divergence of the particle beam in the ToF-AMS as described by Katrib et al. (2004). The particle beam divergence for spherical particles is smaller than for non-spherical particles of the same D_{va}. The particle beam shape is measured by translating a 0.5 mm wire into the particle beam approximately 10 cm from the vaporizer and measuring the resulting decrease in particle transmission as a function of wire location. Figure 6 shows the change in transmission as a function of wire "shadow" on the vaporizer for reacted (OH exposure=8×10^{-8} atm-s) and unreacted BES particles. Because the reaction has no effect on the beam width, we conclude that the BES particles remain spherical after reaction.

The relative changes in particle density and particle volume of reacted BES particles are displayed as a function of OH exposure in Fig. 7. The average density of unreacted BES particles calculated from Eq. (2) is ρ_p=0.91 ($\pm$ 0.02) g cm^{-3}, i.e., within one standard deviation of the material density of liquid BES (ρ=0.915 g cm^{-3}). Figure 7 indicates that the particle densities of reacted BES increased linearly with OH exposure. In contrast, the particle volumes increased slightly at lower OH exposures (V/V$_0$=1.04), then decreased. At the highest OH exposures studied ($\sim$ 9×10^{-8} atm-s), particle density increased by 20% and particle volume decreased by 17%. An increase in particle density was also found for the oxidation of particles coated with oleic acid reacted with O_3 using similar analytical techniques (Katrib et al., 2004). These results suggest that the particles are becoming more oxidized with increasing exposure to OH. Furthermore, volatilization causes a nonlinear decrease in the particle volume, where measurable volume loss is not apparent until BES particles are exposed to 2×10^{-8} atm-s. The effect of O_2 concentration on particle volatilization was investigated by repeating oxidation experiments at OH exposures of 1.1×10^{-9} and 1.4×10^{-8} atm-s with the addition of an O_2 flow to increase the O_2 concentration to near atmospheric levels ([O_2]=3×10^{18}-4×10^{18} molecules cm^{-3}). These experiments showed no difference in volume change relative
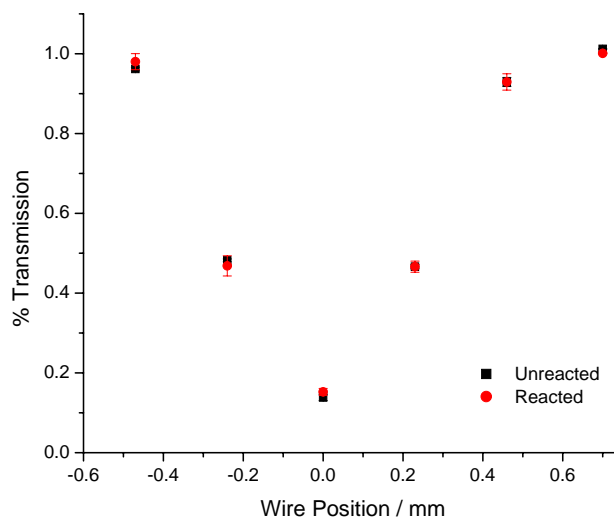

Fig. 6. Particle beam width profile for unreacted (black squares) and reacted (red circles, OH exposure=8.0×10^{-8} atm-s) BES particles.
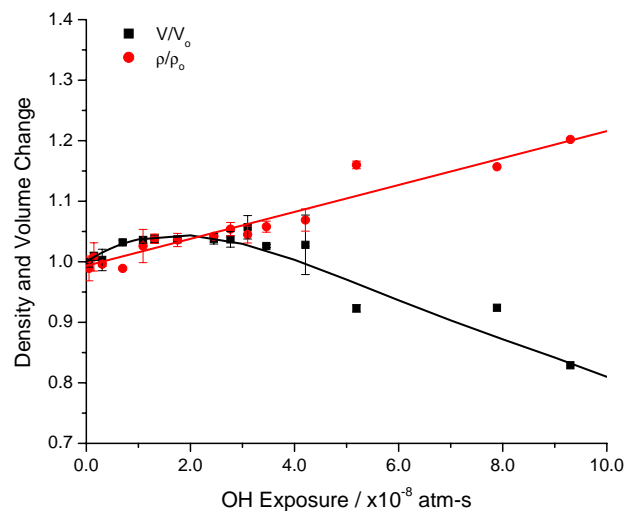

Fig. 7. Relative change in volume (black squares) and density (red circles) of BES particles as a function of OH exposure. Error bars show one standard deviation of averaged data. Lines are fits to guide the eye.

to experiments carried out under similar OH exposures, suggesting that our results are relevant under conditions with atmospheric O_2 concentrations.

3.3 Product identification

Several analytical methods were employed to characterize the oxidation products arising from the reaction of OH with BES particles in order to elucidate the reaction mechanism for this heterogeneous process. We have studied the release of gas-phase products from OH reaction with a BES film using proton-transfer reaction mass spectrometry (PTR-MS),
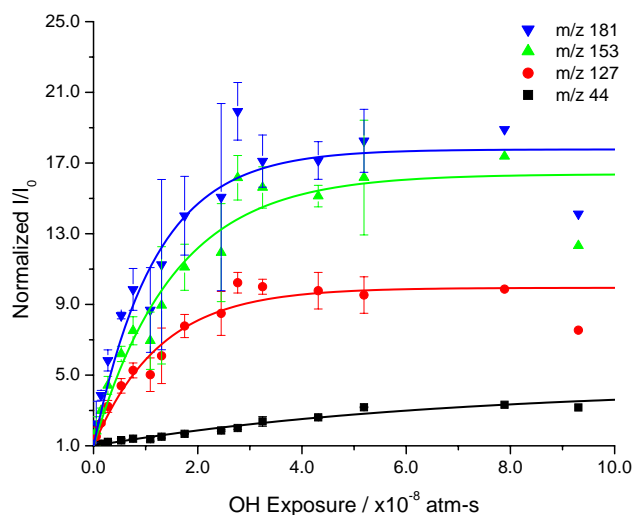
Fig. 8. Kinetic plot for product fragments m/z 44 (black squares), 127 (red circles), 153 (green triangles), and 181 (blue triangles). Error bars show one standard deviation of averaged data. Solid lines are fits to data with the function $y=1+a(1-\exp^{-bx})$.
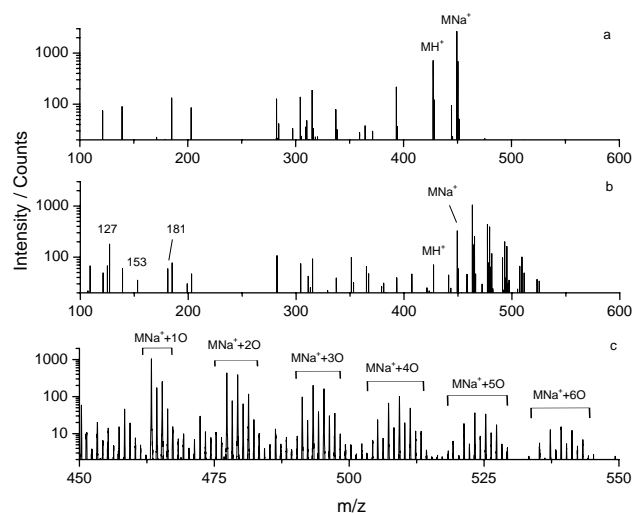

Fig. 9. ESI-MS mass spectra of BES particles: **(a)** unreacted particles, b) reacted particles (OH exposure=2.7×10^{-8} atm-s), c) magnification of panel **(b)** for mass 450 to 550 amu.

which will be presented in a forthcoming paper. Here, we focus on characterization of particle-phase oxidation products. The ToF-AMS provides size-resolved on-line chemical composition information of the particle-phase species. Typical mass spectra of the unreacted and reacted particles taken by ToF-AMS are shown in Fig. 3a and Fig. 3b, respectively. The characteristic mass fragments that are marked in Fig. 3a have clearly decreased in intensity in the reacted particle spectrum in Fig. 3b, whereas several fragments increase in intensity, corresponding to the formation of condensed-

products. The change in the mass spectrum due to OH exposure is shown more clearly in the subtraction spectrum in Fig. 3c. The peaks highlighted in red represent a decrease in the characteristic BES fragments, whereas the green fragments represent an increase in mass intensities, e.g., m/z 44, 127, 153, and 181. The kinetic production of these product fragments was measured as a function of OH exposure as shown in Fig. 8. The kinetic data were fitted to exponential rise to maximum fits. The average kinetic rate constant (k_{avg}) for the product fits for m/z 127, 153, and 181 ($k_{avg}=7.6(\pm1.6)\times10^7$ atm^{-1} s^{-1}) is close to the overall rate constant of decay of m/z 297 ($k_{297}=6.1(\pm0.4)\times10^7$ atm^{-1} s^{-1}), which indicates that these masses are primary product fragments. However, we are not able to determine chemical structures of the product fragments 127, 153, and 181 solely from the ToF-AMS data. The kinetic rate constant for the production of m/z 44 (k_{44}), a mass fragment corresponding to CO_2^+ ion signifying presence of carboxylate groups, was significantly slower ($k_{44}=1.5(\pm0.2)\times10^7$ atm^{-1} s^{-1}) than the values for the other product peaks. This suggests that the oxidized products containing carboxylic groups arise from secondary chemistry and thus form more slowly than primary products. Indeed, there is some indication that the intensities of product masses 127, 153, and 181 decrease at very high OH exposures (greater than 9.0×10^{-8} atm-s) as a result of secondary chemistry.

High molecular weight organic species tend to fragment extensively in the ToF-AMS, and molecular ion peaks are frequently not present in the mass spectrum. Electrospray ionization mass spectrometry (ESI-MS), which uses a softer ionization technique than electron impact, was employed in order to observe the molecular ion peaks of the products and thereby determine the molecular mass of these species. Figure 9 displays the ESI-MS mass spectra of unreacted (Fig. 9a) and reacted (Fig. 9b) BES particles. The two major peaks in Fig. 9a at m/z of 427 (MH$^+$) and 449 (MNa$^+$) both correspond to BES. The stronger signal intensity at MNa$^+$ compared to MH$^+$ is due to the fact that esters are readily sodiated during electrospray ionization (Alex Young, private communication), where the source of Na$^+$ ions may have been from leaching of the glass container holding the extract. The intensities of these BES peaks visibly decreased in the reacted spectrum, while a series of peaks appeared at masses greater than 449 amu in the mass range of 450–550 amu. This area is magnified in Fig. 9c.

We obtained precise masses of the product peaks from the high-resolution ESI-MS measurements, from which we were able to accurately identify chemical compositions of the product peaks. The ESI-MS software (Analyst QS 1.1) was used to identify the most likely chemical composition of each product peak, where the calculated mass of the proposed chemical formula was within a specified error range from the measured peak mass. For example, there were only two proposed chemical formulas for m/z 449 within 10 ppm of the

measured mass, $C_{26}H_{50}O_4Na^+$ (0.37 ppm) and $C_{28}H_{49}O_4$ (5.0 ppm). The first formula corresponds to sodiated BES as expected, which has the lower mass error.

Thus, from analysis of the precise product masses we found that the most likely chemical formulas of the product peaks corresponded to the multiple additions of oxygen atoms in the form of carbonyl or hydroxyl groups, or combinations thereof, in place of CH_2 groups in the BES molecule. For example, the most likely chemical formulas for masses 463 and 465 are $C_{26}H_{48}O_5Na^+$ and $C_{26}H_{50}O_5Na^+$, respectively, which is consistent with the addition of a carbonyl and alcohol, respectively. Furthermore, each set of peaks shown in Fig. 9c moving from lower to higher masses represents the addition of a successive number of oxygen atoms, ranging from 1 to 6 oxygens, in all possible combinations of carbonyls and alcohol groups. Because the BES particles collected for the ESI-MS analysis were exposed to 2.7×10^{-8} atm-s with a corresponding OH to BES ratio of 3, it is not unreasonable that the BES molecules could have reacted with a number of OH radicals to gain more than one oxygenated functional group.

Table 1 summarizes the assigned chemical formulas for the product masses and associated error in calculated mass. We note that we did not quantify the relative ionization efficiencies for BES and particle-phase products. Thus, we cannot accurately compare product yields based on the relative intensities. All assigned formulas, with the exception of peaks with 6 added oxygens, had the lowest or second lowest error of the proposed formulas, where in the second case the formula with the lowest error had several more carbons than BES and thus was deemed an unlikely chemical composition. All errors were within 20 ppm except for the peaks with 6 added oxygens, whose intensities were relatively weak and whose errors were within 100 ppm. Therefore, it is clear from these results that the major condensed phase products are high molecular weight molecules containing carbonyl and alcohol groups. Several product fragments of reacted BES were observed in both the ToF-AMS and ESI-MS mass spectrum, such as m/z 127, 153, and 181. Tandem mass spectrometry (MS/MS) analysis confirmed that the fragments were indeed produced from fragmentation of the protonated product peaks, as the sodiated peaks did not fragment in the mass spectrometer. For example, the major peaks in the MS/MS fragmentation spectrum of m/z 441, the mass corresponding to the protonated form of a major product $C_{26}H_{48}O_5$, included mass fragments 127, 153, and 181. The most likely chemical formulas for product fragments m/z 127, 153, and 181 as determined by precise masses are $C_8H_{15}O^+$, $C_9H_{13}O_2^+$, and $C_{10}H_{13}O_3^+$, respectively. Further MS/MS analysis of these fragment peaks revealed that m/z 153 and 181 had similar fragmentation patterns, whereas m/z 127 had a distinctly different fragmentation pattern. Therefore, m/z 127 likely originates from a different moiety of the product molecule than m/z 153 and 181. The most likely structure for m/z 127 would be a fragment consisting of the

Table 1. Condensed-phase product masses from high resolution ESI-MS analysis of reacted BES particles and proposed chemical formulas. Relative intensities are scaled to the most intense peak at m/z 463. Error in ppm is the fraction of error between calculated and measured masses. Number of added oxygen atoms is expressed as number of added functional groups as carbonyls (C) or alcohols (A).

m/z	Relative Intensity	Chemical Composition	Number of Added Oxygen	Error (ppm)
463.3387	100.0	$C_{26}H_{48}O_5Na^+$	1C	2.7
465.3571	24.4	$C_{26}H_{50}O_5Na^+$	1A	-3.2
477.3258	41.7	$C_{26}H_{46}O_6Na^+$	2C	-13.8
479.3353	37.3	$C_{26}H_{48}O_6Na^+$	1C+1A	-0.9
481.3491	11.2	$C_{26}H_{50}O_6Na^+$	2A	2.9
491.2934	9.3	$C_{26}H_{44}O_7Na^+$	3C	10.3
493.3123	19.2	$C_{26}H_{46}O_7Na^+$	2C + 1A	3.7
495.3254	15.5	$C_{26}H_{48}O_7Na^+$	1C + 2A	8.8
497.3426	3.4	$C_{26}H_{50}O_7Na^+$	3A	5.7
505.272	2.3	$C_{26}H_{42}O_8 Na^+$	4C	11.4
507.2993	6.4	$C_{26}H_{44}O_8 Na^+$	3C + 1A	-11.6
509.3105	9.6	$C_{26}H_{46}O_8 Na^+$	2C + 2A	-2.9
511.3257	4.7	$C_{26}H_{48}O_8 Na^+$	1C + 3A	-2.0
513.3348	1.1	$C_{26}H_{50}O_8 Na^+$	4A	10.8
519.2637	0.6	$C_{26}H_{40}O_9 Na^+$	5C	-12.9
521.2781	1.8	$C_{26}H_{42}O_9Na^+$	4C + 1A	-10.4
523.2964	3.5	$C_{26}H_{44}O_9Na^+$	3C + 2A	-15.5
525.2982	3.2	$C_{26}H_{46}O_9Na^+$	2C +3A	11.0
527.3242	1.7	$C_{26}H_{48}O_9Na^+$	1C + 4A	-8.7
529.3439	0.4	$C_{26}H_{50}O_9Na^+$	5A	-16.3
533.2816	0.2	$C_{26}H_{38}O_{10}Na^+$	6C	-85.0
535.2818	0.5	$C_{26}H_{40}O_{10}Na^+$	5C + 1A	-55.8
537.2856	1.2	$C_{26}H_{42}O_{10}Na^+$	4C +2A	-33.6
539.2725	1.5	$C_{26}H_{44}O_{10}Na^+$	3C + 3A	19.9
541.2942	1.2	$C_{26}H_{46}O_{10}Na^+$	2C + 4A	8.6
543.3093	0.7	$C_{26}H_{48}O_{10}Na^+$	1C +5A	9.6
545.2968	0.3	$C_{26}H_{50}O_{10}Na^+$	6A	61.2

2-ethylhexyl moiety with a carbonyl group on the α-position carbon (i.e., $CH_3(CH_2)_3CH(CH_2CH_3)C(O)^+$). Preferential OH attack of carbon in the α-position of the alkoxy group has been observed by Picquet-Varrault et al. (2002) from gas-phase OH oxidation of isopropyl, isobutyl and tert-butyl acetates. The structures of m/z 153 and 181 are less clear, but it is apparent that m/z 153 results from a loss of CO from the fragment represented by m/z 181. It appears from the MS/MS spectra that these fragments are most likely from the sebacate moiety of the molecule (i.e., $C(O)(CH_2)_8C(O)$) with an addition of an oxygenated functional group to the alkyl chain.

In separate experiments, we have characterized the volatile organic compounds (VOC) that evolved from OH oxidation of a BES film by coated-wall flow tube-CIMS coupled to a
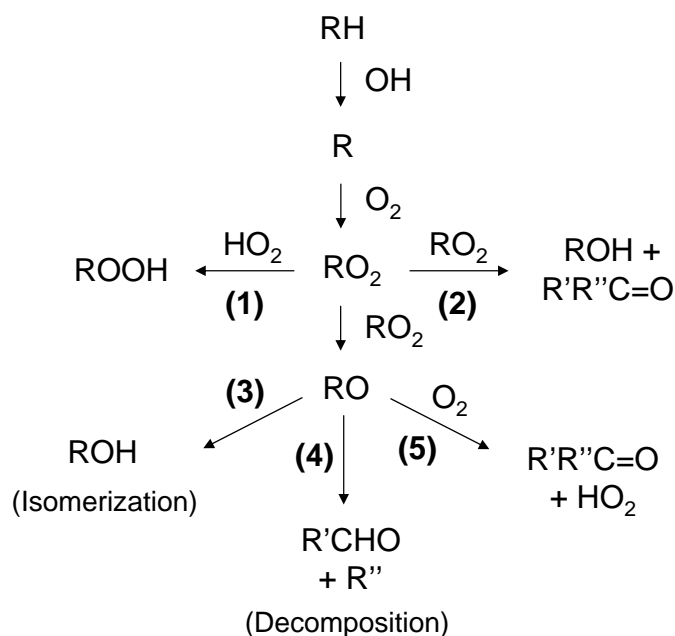
RH

$\downarrow$ OH

R

$\downarrow$ O_2

ROOH $\xleftarrow{\text{HO}_2}$ RO_2 $\xrightarrow{\text{RO}_2}$ ROH +
(1) **(2)** R'R''C=O

$\downarrow$ RO_2

(3) RO O_2

ROH $\xleftarrow{}$ **(4)** **(5)** $\xrightarrow{}$ R'R''C=O
(Isomerization) + HO_2

R'CHO
+ R''
(Decomposition)

Fig. 10. Generalized reaction mechanism for OH-initiated oxidation of a hydrocarbon.

PTR-MS, from which the results will only briefly be touched upon here and will be presented in a future publication. The major gas-phase products from heterogeneous reaction of BES with OH are consistent with the formation of aldehydes and acids ranging in size from 1 to 8 carbons, with a VOC to OH product yield of approximately 10%.

3.4 Reaction mechanism

The reaction mechanism for the heterogeneous oxidation of saturated organic species by OH has been assumed to proceed in a similar manner to the gas-phase reaction mechanism (Atkinson, 1994). A generalized reaction scheme for the reaction of OH with a saturated organic compound has been proposed by other researchers (Molina et al., 2004; Eliason et al., 2004) and is reproduced in Fig. 10 under NO_x-free conditions. The reaction mechanism for gas-phase OH reaction with alkanes has been reviewed in detail by Atkinson (1997) and is summarized below.

Initially, OH abstracts a hydrogen atom from the alkyl chain, producing H_2O and an alkyl radical (R). The alkyl radical R quickly reacts with O_2 in the atmosphere to form RO_2, an alkyl peroxy radical. Alkyl peroxy radicals can self-react through two reaction pathways, leading to the formation of a carbonyl and alcohol (pathway (2)) or to two alkoxy radicals (RO). Alkyl peroxy radicals may also react with HO_2 to form an organic peroxide ROOH (pathway (1)). The branching ratio for pathway (2) leading to formation of a carbonyl + alcohol is approximately 0.3–0.8 in the gas-phase for primary and secondary RO_2 radicals and not

accessible for tertiary RO_2 radicals (Atkinson, 1997). The alkoxy radical (RO) formed from the self-reaction of RO_2 can react by three different pathways: isomerization (pathway (3)), decomposition (pathway (4)), and reaction with O_2 (pathway (5)). RO can isomerize through a 6-membered ring transition-state leading to 1,5 H-shift (pathway (3)) or can react with O_2 to form a carbonyl and HO_2 radical (pathway (5)). Alternatively, the RO radical can decompose through C-C bond scission leading potentially to volatilization of small-chained products (pathway (4)).

We determined from the ESI-MS analysis that OH reaction with BES particles leads to the formation of more oxidized condensed-phase products. These results are supported by the observed increase in particle density with OH exposure. The ESI-MS mass spectra showed that the condensed-phase products consisted of high molecular weight carbonyls and alcohols. It is possible that organic peroxides have formed from the reaction of alkyl peroxy radical with HO_2 (1), but it is unlikely that organic peroxides could have been observed due to their highly unstable nature. The slow increase of the m/z 44 in the ToF-AMS data suggests that carboxylic acids were also being formed, possibly through secondary reactions, e.g., OH-initiated oxidation of aldehydes. It is unlikely that OH would attack the BES terminal carbon leading to formation of a terminal acid with a higher mass than BES. Therefore, the rise in m/z 44 is likely due to shorter-chained acids, which were not observed in the ESI-MS product spectra. The slow kinetics of acid formation and absence of acids in the ESI-MS spectra suggest that acids are not the major condensed-phase products.

This is the first study of its kind to detect both carbonyl and alcohol groups from heterogeneous oxidation of condensed-phase saturated organic species by OH. These results indicate that the channel (2) may be an important pathway. We observed higher signal intensity from the carbonyl product than the alcohol, suggesting that another pathway may be contributing to the formation of the carbonyl product. Because the relative product intensities measured by the ESI-MS are uncalibrated, one should take caution in estimating relative yields from them. High molecular weight carbonyls may also be formed by channel (5). Furthermore, alcohols could be formed from the isomerization of RO (4) and subsequent reaction of the radical to form a hydroxy-substituted carbonyl. This reaction may explain the presence of products containing an addition of both alcohols and carbonyls. Because different reaction pathways lead to carbonyl and alcohol products, the relative importance of each pathway is not clear.

Other studies have also observed oxidized products from the oxidation of condensed-phase saturated organics. For example, Docherty and Ziemann (2006) observed the formation of carbonyl nitrates and alcohol nitrates as oxidation products from the heterogeneous reaction of NO_3 with oleic acid particles. Although the reaction mechanism differs from this study in that the initial step involves addition of NO_3 to the

double bond of an unsaturated organic, it leads nonetheless to the formation of products containing carbonyl and alcohol groups similar to this study. Furthermore, Knopf et al. (2006) observed the formation of alcohol, carbonyl and carboxylic acid groups from XPS measurements of a saturated monolayer oxidized by NO$_3$ radicals, concluding that pathway (2) may potentially be a major pathway in their system. In contrast, Eliason et al. (2004) measured the production of carbonyls but not alcohols from OH oxidation of hexadecane film, and therefore concluded that pathways (4) and (5) were most important. In a recent study, Hearn et al. (2007) investigated the reaction of BES particles with Cl, whereby they estimated product yields of condensed-phase products from this reaction. They also found high molecular weight carbonyls and alcohols to be the major reaction products, which is in agreement with this study. Furthermore, they found that the ratio of the product yields of carbonyls to alcohols to be a function of O$_2$ concentrations. Their study indicates that O$_2$ concentrations will not only affect the reaction rate by controlling the formation rate of RO$_2$, but will also influence the RO + O$_2$ channel as well.

We observed volatilization of oxidation products indirectly from the decrease in particle volume with OH exposure. The relative importance of the RO decomposition pathway to the pathways leading to the formation of high molecular weight carbonyl and alcohols was examined by comparing observed particle mass changes to predicted mass change from the formation of condensed and gaseous oxidation products . For this calculation, we assumed a product yield for the formation of volatile compounds of 10% with an average product molecular weight of 58 amu. These assumptions are based on unpublished work by our group, in which the masses and product yields of volatile organics from OH oxidation of BES film were determined by use of coated-wall flow tube coupled to a PTR-MS. We also assumed that carbonyls and alcohols were formed in equal amounts such as in pathway (2) as a simplified case and that the particle density did not change from volatilization. Therefore, 1 of every 10 OH collisions with a BES particle will lead to the loss of 58 amu from a BES molecule. We assumed that the other 9 collisions out of 10 (γ=1) lead to the formation of alcohol or carbonyl groups with average mass addition of 15 amu to BES molecule for each collision leading to this pathway.

Figure 11 shows the observed and predicted particle mass changes as a function of OH exposure based on the assumptions explained above. The observed particle mass changes were determined from the density and volume measurements. The red and blue lines represent the relative contributions to mass change from the carbonyl + alcohol pathway (2) with a product yield of 90% and decomposition pathway (4) with product yield of 10%, respectively. The pink line represents the overall predicted mass change from the two contributions stated, which indicates that the particle mass should increase linearly with OH exposure up to 10%. The observed particle mass does not however change linearly with OH ex-
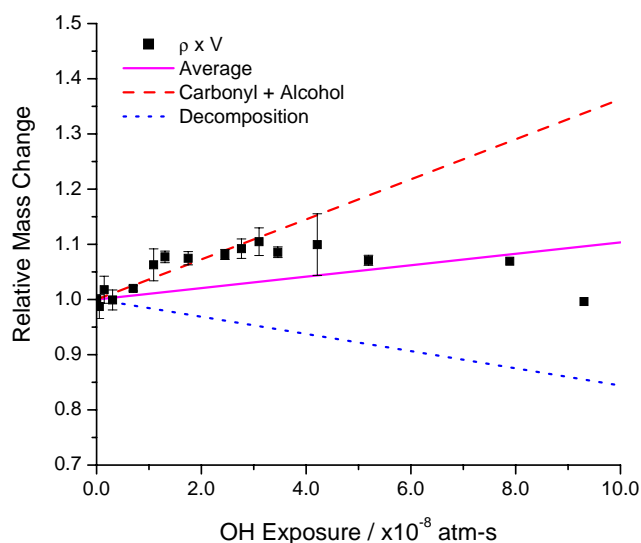

Fig. 11. Relative particle mass change as a function of OH exposure. Black squares are calculated mass values from the product of density and volume measurements, red dashed and blue dotted lines show theoretical contribution of carbonyl + alcohol and decomposition reaction pathways to mass change, respectively, assuming a VOC/OH ratio of 0.1 and average VOC molecular mass of 58 g mol^{-1}, and pink line shows theoretical overall mass change (See text).

posure. At OH exposures below 3×10^{-8} atm-s, the particle mass increases to approximately 10% following the trend for the carbonyl + alcohol contribution. At higher OH exposures, the particle mass then decreases to no net mass change. This observation suggests that the volatilization contribution to the particle mass change is not linear. One possible explanation for nonlinear volume change is that at higher OH exposures the condensed-phase products gain more functional groups, so as the products react with OH they decompose more readily through channel (4) than BES. These results indicate that the particle mass change contributions from the formation of condensed-phase and volatile products cancel out to some degree, with 10% maximum change in particle mass. In this study, volatilization of products from pathway (4) was found to be a minor reaction pathway in the OH oxidation of BES particles under our experimental conditions. Our study is in contrast to the recent study by Molina et al. (2004), who observed complete volatilization of an alkane monolayer for an OH exposure of 3 OH collisions per alkane molecule. At the same OH exposure (i.e., 2.6×10^{-8} atm-s), we did not see any evidence of volatilization. It is possible that because BES has a longer chain and higher molecular weight than the alkane monolayer studied by Molina et al. (2004) BES may require more OH collisions for decomposition products to volatilize. Under our experimental conditions, particles would completely volatilize only if the VOC formation to OH loss product ratio was 0.7 or higher. The

studies by Knopf et al. (2006) and Moise and Rudich (2001) are more in line with our results. Knopf et al. (2006) found that NO₃ reaction with an alkane monolayer lead to a small amount (up to 10%) of volatilization of the surface carbon. Furthermore, Moise and Rudich (2001) measured up to 20% loss of carbon from the oxidation of alkane monolayers by Cl and Br radicals. Although NO₃, OH and halogen radicals should react with organics by a mechanism similar to that shown in Fig. 10, these studies suggest that the importance of the pathways for RO may depend sensitively on specific experimental conditions.

One major difference between these studies and ours is that we have studied the reaction using liquid aerosol particles as opposed to monolayers on a solid substrate or solid films. It has been suggested that the particle phase may influence the reaction pathways (Knopf et al., 2006; Docherty and Ziemann, 2006), with channel (2) suggested as being the dominant reaction pathway for liquid organics (Russell, 1957). Eliason et al. (2004) detected small-chained products from the reaction of a thin liquid hexadecane film with OH in the condensed-phase only, but did not detect products in the gas phase. Their results indicate that decomposition is an important pathway for oxidation liquid organic species by OH, but it is unclear to what extent compared to the other pathways. The results in our study clearly show that for liquid organic aerosols, the pathways leading to the production of carbonyls and alcohols, i.e., pathways (2), (3) and (5) are more important than the decomposition pathway. The same conclusion may not hold, however, for solid organic particles, which will require further study.

It is possible that the reaction mechanism for OH oxidation of organic aerosols may be influenced by experimental conditions. For example, recent work by Hearn et al. (2007) confirmed that pathway (5) is affected by O₂ concentrations as expected. It is possible that as O₂ concentration is reduced, RO decomposition may be favored over reaction with O₂. Note that we did not see an enhancement of volatilization at O₂ concentrations two orders of magnitude lower than atmospheric levels. The chemical composition of the model organic compound, such as degree of oxidation, chain length and degree of branching, may also influence the reaction mechanism. For example, the branching ratio for pathway (2) may be reduced during the oxidation of branched organic compounds such as BES compared to unbranched compounds as the mechanism requires an H-atom transfer (Russell, 1957). Under the NOₓ-free conditions in this study, it is likely that pathway (2) is enhanced compared to the RO₂ self-reaction leading to RO formation. The presence of NOₓ may lead to increased yields of RO formation, thus reducing the yield of the carbonyl + alcohol (2) channel and perhaps leading to nitrated products. The influence of these experimental factors on the OH-initiated reaction mechanism should be systematically studied in the future.

4 Atmospheric implications and conclusions

In this work, we investigated the heterogeneous oxidation of BES particles by OH under NOₓ-free conditions. These conditions were chosen as a simplified case simulating remote atmospheric conditions. The oxidation of organic aerosol by OH is highly efficient with a reactive coefficient of $\gamma \approx 1$ for the reaction of OH with BES particles. This study serves as a simple model for the chemical aging of atmospheric aerosols in the troposphere containing saturated organic matter, such as primary organic aerosol, organic coatings on marine aerosol, biomass burning aerosol and secondary organic aerosol (SOA) formed from photochemical oxidation of volatile organics (Finlayson-Pitts and Pitts, 2000). Although studies with more chemically complex particles are required, this system can be useful as an initial proxy for saturated organic aerosol in the troposphere.

This study suggests that chemical aging of organic aerosol by OH has an important impact on the physical and chemical properties of tropospheric organic aerosol. We observed the accumulation of oxidized products in the condensed phase from the heterogeneous oxidation of BES particles. Several recent field studies have observed a greater degree of oxidation of ambient organic aerosols with an increase in photochemical age (de Gouw et al., 2005; McFiggans et al., 2005; Takegawa et al., 2006). Moreover, Robinson et al. (2006) discovered evidence for chemical oxidation of tropospheric organic aerosol during regional transport, especially during the summer.

To determine the importance of heterogeneous oxidation of atmospheric organic aerosol by OH relative to the lifetime of atmospheric organic aerosols, we calculated the oxidation lifetime (τ) of a model tropospheric organic particle in a manner similar to that presented in Robinson et al. (2006). For this calculation, we assumed a 24-h averaged OH concentration of [OH]=10^6 cm^{-3} and that γ=1 for reactive uptake of OH onto a model particle with a radius R=50 nm containing saturated hydrocarbons with an average molecular weight of M=300 g mol^{-1}. The oxidation lifetime of the model organic aerosol is defined as the time needed for every organic molecule initially present in the aerosol to be oxidized by one OH radical (Robinson et al., 2006). As with our kinetic calculations, we assume that the rate of reactive uptake of OH equals the rate of oxidation of the hydrocarbon molecules and that the hydrocarbons are equally mixed throughout the particle. The latter assumption is reasonable as the diffusion time of a hydrocarbon in a particle with a diameter of 100 nm with an assumed diffusion coefficient of D∼10^{-6} cm^2 s^{-1} was calculated to be 30 μs. Under the given assumptions, we calculated the oxidation lifetime of an organic particle as the number of initial hydrocarbon molecules in the particle (N) divided by the reactive flux of OH into the particle (J) using the equation given in Robinson et al. (2006):

$$\tau = \frac{N}{J} = \frac{\frac{4}{3}\pi R^3 \frac{\rho N_a}{M}}{\gamma \pi R^2 \bar{c}[\text{OH}]} = \frac{4}{3} R \frac{\rho N_a}{\gamma \bar{c}[\text{OH}]M} \quad (3)$$

Here, $\bar{c}$ is the average thermal speed of OH and ρ is the particle density assumed to be $\rho \sim 1\,\text{g cm}^{-3}$. From Eq. (3) we calculated an oxidation lifetime of 2.6 days, which is consistent with the oxidation lifetime calculated by Robinson et al. (2006).

This simple calculation suggests that organic aerosol can be significantly oxidized within the typical lifetime of an atmospheric particle of approximately 5 to 10 days (Kanakidou et al., 2005). Therefore, OH oxidation may be an important mechanism for the chemical transformation of tropospheric organic aerosol in the time scale of regional transport and less important for local urban organic aerosol sources (Zhang et al., 2005). The oxidation lifetime may strongly depend on the chemical composition and phase of the atmospheric particles and the ability of the organic molecules to diffuse to the particle surface. Furthermore, organic molecules that preferentially partition to the surface, e.g. organic coatings on aqueous aerosols, will be oxidized more rapidly than organics in the bulk phase.

In this study, we observed the production of high molecular weight carbonyls and alcohols as the major particle-phase products. Recent smog chamber studies of SOA formation have indicated that heterogeneous oligomerization reactions may explain the observed increase in SOA mass compared to expected SOA formation (i.e., Jang et al., 2002, Kalberer et al., 2004; Baltensperger et al., 2005). Heterogeneous oxidation of organic particles by OH is another mechanism to increase organic aerosol mass in the atmosphere as well as increase the degree of oxidation. An increase in oxidized particle-phase species may influence the hygroscopic properties of the particles and their ability to act as cloud condensation nuclei. Heterogeneous oxidation of aerosols will result in an increase the density of the aerosols, as observed in our studies, as well as alter their optical properties. Although we found evidence for the formation of volatile oxidation products by observing the loss of particle volume up to 17%, the reaction pathway leading to release of volatile products was a minor one from a mass-weighted perspective. Kwan et al. (2006) evaluated the importance of photochemical oxidation of organic aerosols as a source of oxidized VOC. Their calculations suggest that this process may be an important source of oxidized VOC based on the work by Molina et al. (2004) assuming each OH collision leads to the loss of one VOC consisting of 6 carbons. Our study suggests that the calculated VOC flux from aerosol oxidation may not be as important if the VOC yield from liquid organic aerosols is lower than that for solid aerosols.

It should be noted that extrapolation of laboratory results to ambient conditions may be problematic if the kinetics or mechanism of chemical aging of organic aerosol are influenced by the complexity of the chemical matrix that make up the aerosol particles or the concentration of oxidants. The particle phase may have a significant impact on the chemical transformation of organic aerosol. This has been shown to be true for the heterogeneous chemistry of O_3 with organic aerosol containing oleic acid. Several researchers have found that mixtures of liquid unsaturated oleic acid with solid saturated organic species, such as stearic acid, may slow the kinetics of chemical aging (Katrib et al., 2005; Hearn and Smith, 2005; Knopf et al., 2005). These results may explain the discrepancy in the short lifetime of oleic acid predicted by experimental data and the much longer lifetimes measured in ambient conditions. It is also important to validate that the same heterogeneous kinetics and reaction mechanism apply at lower oxidant concentrations that are more similar to ambient conditions. Thus, it is vital not only to study the particle morphology and phase of ambient organic aerosol, but also to focus future laboratory studies on investigating chemical aging of more complex aerosol systems with experimental conditions that more closely mimic atmospheric conditions.

Edited by: D. Cziczo

References

Alfarra, M. R.: Insights into Atmospheric Organic Aerosols Using an Aerosol Mass Spectrometer, Ph.D. Dissertation thesis, University of Manchester, Manchester, 2004.

Atkinson, R.: Gas-phase tropospheric chemistry of organic compounds, J. Phys. Chem. Ref. Data Monograph, 2, 1–216, 1994.

Atkinson, R.: Gas-phase tropospheric chemistry of volatile organic compounds. 1. Alkanes and alkenes, J. Phys. Chem. Ref. Data, 26, 215–290, 1997.

Baltensperger, U., Kalberer, M, Dommen, J., Paulsen, D., Alfarra, M. R., Coe, H., Fisseha, R., Gascho, A., Gysel, M., Nyeki, S. Sax, M., Steinbacher, M., Prevot, A. S. H., Sjögren, S., Weingartner, E., and Zenobib, R.: Secondary organic aerosols from anthropogenic and biogenic precursors, Faraday Discuss., 130, 265–278, 2005.

Bertram, A. K., Ivanov, A. V., Hunter, M., Molina, L. T., and Molina, M. J.: The reaction probability of OH on organic surfaces of tropospheric interest, J. Phys. Chem. A, 105, 9415–9421, 2001.

Braun, W, Herron, J. T., and Kahaner, D. K.: Acuchem – A computer-program for modeling complex chemical-reaction systems, Int. J. Chem. Kinet., 20, 51–62, 1988.

Cooper, P. L. and Abbatt, J. P. D.: Heterogeneous interactions of OH and HO_2 radicals with surfaces characteristic of atmospheric particulate matter, J. Phys. Chem., 100, 2249–2254, 1996.

de Gouw, J. A., Middlebrook, A. M., Warneke, C., Goldan, P. D., Kuster, W. C., Roberts, J. M., Fehsenfeld, F. C., Worsnop,

D. R., Canagaratna, M. R., Pszenny, A. A. P., Keene, W. C., Marchewka, M., Bertman, S. B., and Bates, T. S.: Budget of organic carbon in a polluted atmosphere: Results from the New England Air Quality Study in 2002, J. Geophys. Res.-Atmos., 110, D16305, doi:10.1029/2004JD005623, 2005.

DeCarlo, P., Slowik, J. G., Worsnop, D. R., Davidovits, P., and Jimenez, J. L.: Particle morphology and density characterization by combined mobility and aerodynamic diameter measurements. Part 1: Theory, Aerosol Sci. Technol., 38, 1185–1205, 2004.

DeMore, W. B., Sander, S. P., Golden, D. M., Hampson, R. F., Kurylo, M. J., Howard, C. J., Ravishankara, A. R., Kolb, C. E., and Molina, M. J.: Chemical kinetics and photochemical data for use in stratospheric modelling, Evaluation No. 12, JPL Publication 97-4, 1997.

Docherty, K. S. and Ziemann, P. J.: Reaction of oleic acid particles with NO_3 radicals: Products, mechanism, and implications for radical-initiated organic aerosol oxidation, J. Phys. Chem. A, 110, 3567–3577, 2006.

Drewnick, F., Hings, S. S., DeCarlo, P., Jayne, J. T., Gonin, M., Fuhrer, K., Weimer, S., Jimenez, J. L., Demerjian, K. L., Borrmann, S., and Worsnop, D. R.: A new time-of-flight aerosol mass spectrometer (TOF-AMS) - Instrument description and first field deployment, Aerosol Sci. Technol., 39, 637–658, 2005.

Eliason, T. L., Gilman, J. B., and Vaida, V.: Oxidation of organic films relevant to atmospheric aerosols, Atmos. Environ., 38, 1367–1378, 2004.

Finlayson-Pitts, B. J. and Pitts, J. N.: Chemistry of the Upper and Lower Atmosphere: Theory, Experiments, and Applications, Academic Press, 2000.

Fuchs, N. A. and Sutugin, A. G.: Highly Dispersed Aerosols, Ann Arbor Science Publishers, 1970.

Hearn, J. D. and Smith, G. D.: Kinetics and product studies for ozonolysis reactions of organic particles using aerosol CIMS, J. Phys. Chem. A, 108, 10 019–10 029, 2004.

Hearn, J. D. and Smith, G. D.: Measuring rates of reaction in supercooled organic particles with implications for atmospheric aerosol, Phys. Chem. Chem. Phys., 7, 2549–2551, 2005.

Hearn, J. D. and Smith G. D.: A mixed-phase relative rates technique for measuring aerosol reaction kinetics, Geophys. Res. Lett., 33, L17805, doi:10.1029/2006GL026963, 2006.

Hearn, J. D., Renbaum, L. H., Wang, Xi, and Smith, G. D.: Kinetics and products from reaction of Cl radicals with dioctyl sebacate (DOS) particles in O_2: a model for radical-initiated oxidation of organic aerosols, Phys. Chem. Chem. Phys., 2007, doi:10.1039/b707523e.

Ivanov, A. V., Trakhtenberg, S., Bertram, A. K., Gershenzon, Y. M., and Molina, M. J.: OH, HO_2, and ozone gaseous diffusion coefficients, J. Phys. Chem. A, 111, 1632–1637, 2007.

Jacobson, M. C., Hansson, H. C, Noone, K. J., and Charlson, R. J.: Organic atmospheric aerosols: Review and state of the science, Rev. Geophys., 38, 267–294, 2000.

Jang, M., Czoschke, N. M., Lee, S., and Kamens, R. M.: Heterogeneous atmospheric aerosol production by acid-catalyzed particle-phase reactions, Science, 298, 814–817, 2002.

Kalberer, M., Paulsen, D., Sax, M., Steinbacher, M., Dommen, J., Prevot, A. S. H., Fisseha, R., Weingartner, E., Frankevich, V., Zenobi, R., and Baltensperger, U.: Identification of polymers as major components of atmospheric organic aerosols, Science, 303, 1659–1662, 2004.

Kanakidou, M., Seinfeld, J. H., Pandis, S. N., Barnes, I., Dentener, F. J., Facchini, M. C., Dingenen, R. V., Ervens, B., Nenes, A., Nielsen, C. J., Swietlicki, E., Putaud, J. P., Balkanski, Y., Fuzzi, S., Horth, J., Moortgat, G. K., Winterhalter, R., Myhre, C. E. L., Tsigaridis, K., Vignati, E., Stephanou, E. G., and Wilson, J.: Organic aerosol and global climate modelling: a review, Atmos. Chem. Phys., 5, 1053–1123, 2005, http://www.atmos-chem-phys.net/5/1053/2005/.

Katrib, Y., Martin, S. T., Hung, H. M., Rudich, Y., Zhang, H. Z., Slowik, J. G., Davidovits, P., Jayne, J. T., and Worsnop, D. R.: Products and mechanisms of ozone reactions with oleic acid for aerosol particles having core-shell morphologies, J. Phys. Chem. A, 108, 6686–6695, 2004.

Katrib, Y., Biskos, G., Buseck, P. R., Davidovits, P., Jayne, J. T., Mochida, M., Wise, M. E., Worsnop, D. R., and Martin, S. T.: Ozonolysis of mixed oleic-acid/stearic-acid particles: Reaction kinetics and chemical morphology, J. Phys. Chem. A, 109, 10 910–10 919, 2005.

Knopf, D. A., Anthony, L. M., and Bertram, A. K.: Reactive uptake of O_3 by multicomponent and multiphase mixtures containing oleic acid, J. Phys. Chem. A, 109, 5579–5589, 2005.

Knopf, D. A., Mak, J., Gross, S., and Bertram, A. K.: Does atmospheric processing of saturated hydrocarbon surfaces by NO_3 lead to volatilization?, Geophys. Res. Lett., 33, L17816, doi:10.1029/2006GL026884, 2006.

Kwan, A. J., Crounse, J. D., Clarke, A. D., Shinozuka, Y., Anderson, B. E., Crawford, J. H., Avery, M. A., McNaughton, C. S., Brune, W. H., Singh, H. B., and Wennberg, P. O.: On the flux of oxygenated volatile organic compounds from organic aerosol oxidation, Geophys. Res. Lett., 33, L15815, doi:10.1029/2006GL026144, 2006.

Lambe, A. T., Zhang, J., Sage, A. M., and Donahue, N. M.: Controlled OH radical production via ozone-alkene reactions for use in aerosol aging studies, Environ. Sci. Technol., 41, 2357–2363, 2007.

Massman, W. J.: A review of the molecular diffusivities of H_2O, CO_2, CH_4, CO, O_3, SO_2, NH_3, N_2O, NO, and NO_2 in air, O_2 and N_2 near STP, Atmos. Environ., 32, 1111–1127, 1998.

McFiggans, G., Alfarra, M. R., Allan, J., Bower, K., Coe, H., Cubison, M., Topping, D., Williams, P., Decesari, S., Facchini, C., and Fuzzi, S.: Simplification of the representation of the organic component of atmospheric particulates, Faraday Discuss., 130, 341–362, doi:10.1039/b419435, 2005.

Moise, T. and Rudich, Y.: Uptake of Cl and Br by organic surfaces - a perspective on organic aerosols processing by tropospheric oxidants, Geophys. Res. Lett., 28(21), 4083–4086, 2001.

Moise, T. and Rudich, Y.: Reactive uptake of ozone by aerosol-associated unsaturated fatty acids: Kinetics, mechanisms and products, J. Phys. Chem. A, 106, 6469–6476, 2002.

Moise, T., Talukdar, R. K., Frost, G. J., Fox, R. W., and Rudich, Y.: Reactive uptake of NO_3 by liquid and frozen organics, J. Geophys. Res., 107(D2), 4014, doi:10.1029/2001JD000334, 2002.

Molina, M. J., Ivanov, A. V., Trakhtenberg, S., and Molina, L. T.: Atmospheric evolution of organic aerosol, Geophys. Res. Lett., 31, L22104, doi:10.1029/2004GL020910, 2004.

Morris, J. W., Davidovits, P., Jayne, J. T., Jimenez, J. L., Shi, Q., Kolb, C. E., Worsnop, D. R., Barney, W. S., and Cass, G.: Kinetics of submicron oleic acid aerosols with ozone: A novel aerosol mass spectrometric technique, Geophys. Res. Lett., 29(9), 1357,

doi:10.1029/2002GL014692, 2002.

Picquet-Varrault, B., Doussin, J.-F., Durand-Jolibois, R., and Carlier, P.: FTIR spectroscopic study of the OH-induced oxidation of isopropyl, isobutyl, and *tert*-butyl acetates, J. Phys. Chem. A, 106, 2895–2902, 2002.

Ramanathan, V., Crutzen, P. J., Kiehl, J. T., and Rosenfeld, D.: Aerosols, climate, and the hydrological cycle, Science, 294, 2119–2124, 2001.

Robinson, A. L., Donahue, N. M., and Rogge, W. F.: Photochemical oxidation and changes in molecular composition of organic aerosol in the regional context, J. Geophys. Res., 111, D03302, doi:10.1029/2005JD006265, 2006.

Russell, G. A.: Deuterium-isotope effects in the autooxidation of aralkyl hydrocarbons: Mechanism of the interaction of peroxy radicals, J. Am. Chem. Soc., 79, 3871–3877, 1957.

Saxena, P. and Hildemann, L. M.: Water-soluble organics in atmospheric particles: A critical review of the literature and application of thermodynamics to identify candidate compounds, J. Atmos. Chem., 24, 57–109, 1996.

Seinfeld, J. H. and Pandis, S. N.: Atmospheric Chemistry and Physics: From Air Pollution to Climate Change, Wiley-Interscience, 1998.

Takegawa, N., Miyakawa, T., Kondo, Y., Blake, D. R., Kanaya, Y., Koike, M., Fukuda, M., Komazaki, Y., Miyazaki, Y., Shimono, A., and Takeuchi, T.: Evolution of submicron organic aerosol in polluted air exported from Tokyo, Geophys. Res. Lett., 33, L15814, doi:10.1029/2006GL025815, 2006.

Thornberry, T. D. and Abbatt, J. P. D.: Heterogeneous reaction of ozone with liquid unsaturated fatty acids: Detailed kinetics and gas-phase product studies, Phys. Chem. Chem. Phys., 6, 84–93, 2004.

Worsnop, D. R., Morris, J. W., Shi, Q., Davidovits, P., and Kolb, C. E.: A chemical kinetic model for reactive transformations of aerosol particles, Geophys. Res. Lett., 29(20), 1357, doi:10.1029/2002GL015542, 2002.

Zhang, Q., Worsnop, D. R., Canagaratna, M. R., and Jimenez, J. L.: Hydrocarbon-like and oxygenated organic aerosols in Pittsburgh: Insights into sources and processes of organic aerosols, Atmos. Chem. Phys., 5, 3289–3311, 2005, http://www.atmos-chem-phys.net/5/3289/2005/.

Ziemann, P. J.: Aerosol products, mechanisms, and kinetics of heterogeneous reactions of ozone with oleic acid in pure and mixed particles, Faraday Discuss., 130, 469–490, 2005.